Study of Crater Structure Formation on the Surface of Biaxially Oriented Polypropylene Film

Satoshi Tamura,[1] Katsutoshi Ohta,[1] Toshitaka Kanai[2]

[1]*Research and Development Division, Prime Polymer Co., Ltd., 580-30, Nagaura, Sodegaura-City, Chiba, 299-0265 Japan*
[2]*Performance Materials Laboratories, Idemitsu Kosan Co., Ltd., 1-1, Anesaki-Kaigan, Ichihara-City, Chiba, 299-0193, Japan*

Received 31 December 2010; accepted 1 June 2011
DOI 10.1002/app.35115
Published online 3 November 2011 in Wiley Online Library (wileyonlinelibrary.com).

ABSTRACT: Biaxially oriented polypropylene (BOPP) film accounts for a large amount of polypropylene since it is well suited for food packaging films or industrial films, because of its high performance in terms of mechanical and optical properties. Recently machine speed has been increasing to obtain higher production rate and film thickness has become thinner to reduce the environmental load. To meet the demands, many researchers have been investigating stretchability of PP by connecting the stretching force at the yield point and crystalline structure. Many other studies have been conducted regarding the surface structure of BOPP. Although there were some cases that crater-like film surface roughness was formed on BOPP films, the formation mechanism of craters has not been clarified. In this report, new hypothesis of the crater-like film surface roughness formation mechanism is proposed by observing the transformation of crater from sheet to BOPP film and by investigating the relationship between the stress–strain curve and surface roughness change. © 2011 Wiley Periodicals, Inc. J Appl Polym Sci 124: 2725–2735, 2012

Key words: films; orientation; polypropylene (PP); surfaces

INTRODUCTION

About 40 million tons of polypropylene (PP) is currently produced per year in the world.[1] Compared with PET which has a low crystallizing speed, PP is difficult to stretch because PP has a higher stretching force at the yield point due to a high crystalline speed.[2] In addition to studies on stretchability and crystallinity of BOPP films, various researches have reported regarding the surface structure of BOPP films.[3–9] Since β crystals with lower density in PP sheet change into α crystals with a higher density after stretching the sheet which contains both α and β crystals, the formation of crater-like film surface roughness of BOPP films was reported as being formed by the difference between the densities of α and β crystals with crystal dislocation system.

α crystal structure has been analyzed by Natta and Corradini in 1960, and now it is known as being the most dominant crystal in PP, and its unit lattice is the monoclinic system.[10] β crystal is a semisteady system of crystal discovered by Keith in 1959, and the unit lattice is a hexagonal system.[11] It was reported that the β crystal can be easily formed under special conditions, for example, by adding the β nucleating agent,[12] and crystallizing under a certain temperature gradient,[13] or under a strong shear stress.[14] Furthermore, in addition to density of the β crystal being lower than that of the α crystal, it is a well known fact that the β crystal has low melting point, slow nucleation, and high growth speed.

The surface structure control technology of BOPP film using the crystal dislocation system from β crystal to α crystal has been used for a long time. Fujiyama et al. reported that the β crystal content in a sheet with a thickness of 600 μm became higher by adding more β crystal nucleator and casting under a lower extruder temperature.[3] In addition to that, it has been reported that the surface roughness of BOPP films can be easily formed by controlling the machine direction (MD) stretching temperature between a β crystal melting point and an α crystal melting point,[4] and also by controlling transverse direction (TD) stretching temperatures from 150 to 155°C using PP of melt flow rate (MFR) at around 8 g/min.[5] Furthermore, Fujiyama et al. reported the difference of the film surface structure between BOPP films with α nucleator and that with β nucleator,[6] the relationship between the β crystal size of the sheet and the surface crater size of BOPP film,[7] the comparison of the crater shape between a multilayer sheet and a mono-layer sheet,[8] and the influence on crater shape when low melting point resins were blended.[9]

However, the formation mechanism of the crater of BOPP film from the sheet is not yet to be explained. Therefore, this report will give some

Correspondence to: S. Tamura (Satoshi1.Tamura@primepolymer.co.jp).

perspective on the formation mechanism of crater, like roughness of BOPP films obtained by the careful observation of the transforming behavior on the surface of the sheet and BOPP films. Furthermore, the importance of crater shape is also reported.

EXPERIMENTS

Samples

To clarify the mechanism of the formation of the surface craters, two PP resins with different tacticity, PP-A, and PP-B were prepared. PP-A has a high tacticities with meso pentad value mmmm of 96mol% which is a parameter of isotactic index measured in ^{13}C-NMR and, PP-B has a low tacticity with mmmm value of 91 mol %. Their MFRs were 3.5 g/10 min and 3.0 g/10 min, respectively. Properties of PP-A and PP-B are shown in Table I. Melting point of PP-A was 3°C higher than that of PP-B, because stereoregularity of PP-A is higher than PP-B.

PP sheets were produced using a sheet forming machine (GM Engineering) with φ35 mm extruder (Fig. 1). PP resins were extruded from a die with a width of 200 mm at 250°C. Then PP resins were cast by a chill-roll with a diameter of φ25 mm at 1 revolution per minute and PP sheets with a thickness of 500 μm were produced at various chill-roll temperatures.

After the PP sheet was cut into a sheet with a length and width of 85 mm by 85 mm, the PP square sheet was stretched by a table tenter (Bruckner KARO IV). BOPP film was obtained at an arbitrary stretching temperature and stretching ratio after PP sheet was preheated for 1 min. A stretching force was measured by a load cell which was equipped on a chuck of a table tenter at several temperatures and at constant strain speed of 143%/s to connect with the formation mechanism of crater-like roughness of BOPP.

Evaluation of PP sheets and the BOPP films

The surface structure of PP sheets and the BOPP films were observed by SEM (JOEL JSM5600LV). In addition, the shapes of the craters were measured by a highly precise shape measuring machine (Kosaka Laboratory SURFCODER ET4000A) using a diamond head at head pressure of 70 μ*N*.

TABLE I
Properties of PP Resin

Properties	Unit	PP-A	PP-B
MFR	g/10 min	3.5	3.0
mmmm	mol %	96	91
T_m	°C	164	161
T_c	°C	113	112
M_w/M_n	–	5.1	4.5

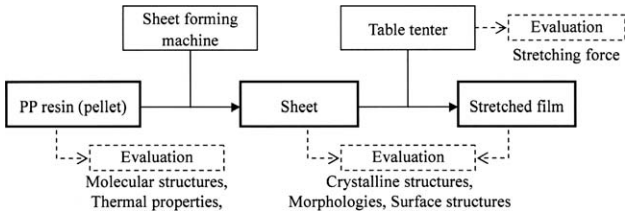

Figure 1 Diagram of sample producing and evaluation of each sample.

The sectional and surface structures of PP sheets and the BOPP films were observed by an optical microscope (Nikon ECLIPSE-LV100POL), and SEM (JOEL JSM5600LV). On observing the PP sheet sectional structure using an optical microscope, crystal sizes were measured by visual inspection from pictures taken with polarizing lens. On observing the surface structure using SEM, sample was sputtered with gold in vacuumed atmosphere. On observing the cross-sectional view of sample at several stretching ratio, sample was buried into epoxy resin and waited until it was solidified to avoid crumbling. Afterward, the sample was cut at room temperature to observe its cross section.

X-ray diffractions were measured on the PP sheets and the BOPP films with a Rigaku Denki RINT-2500 diffractometer with Ni-filtered Cu-Kα radiation. The β crystal content named as the K-value was calculated from the diffraction curves shown in Figure 2 according to the eq. (1) proposed by Tuner Jones.[15] In addition, crystallinity χ_C of PP sheets which is an index of the quantity of the crystal part was calculated from the diffraction curves in Figure 2 according to the eq. (2) proposed by Giulio Natta.[16]

$$K = \frac{H\beta 1}{H\beta 1 + H\alpha 1 + H\alpha 2 + H\alpha 3} \quad \cdots \qquad (1)$$

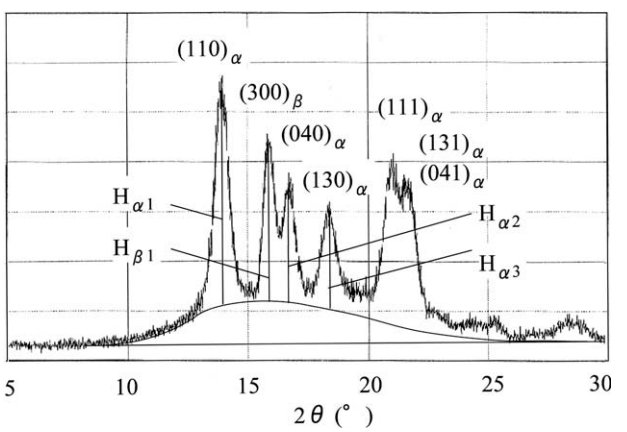

Figure 2 WAXD Pattern of PP sheet and evaluation of β-form crystal ratio (*K* values).

TABLE II
Properties of PP Sheet

Properties		Unit	A30-500	A80-500	B30-500	B80-500
PP resin		–	A	A	B	B
Chill-roll temperature		°C	30	80	30	80
Thickness		μm	500	500	500	500
χ_C		%	46	65	48	64
K		–	<0.01	0.08	0.00	<0.01
Chill-roll side	Ra	μm	0.08	0.07	0.05	0.05
	Rz	μm	0.21	0.26	0.20	0.21
	Gloss	%	93	88	94	91
Opposite side of chill-roll	Ra	μm	0.51	0.66	0.36	0.42
	Rz	μm	2.24	2.85	1.63	1.90
	Gloss	%	44	31	53	46

Ra, arithmetic mean roughness; Rz, ten points average roughness (JIS B0601[1994]).

Where Hβ1, Hα1, Hα2, and Hα3 are the reflection intensities of the (300) plane of β crystals, (110), (040), and (130) planes of α crystals, respectively.

$$\chi_c = \frac{I_c}{I_c + 6.21 \times I_a} \quad (2)$$

Where I_c is total area of crystal part and I_a is total area of amorphous part.

RESULTS AND DISCUSSION

The relationship between the crystalline structure of sheet and crater shape of BOPP film surface

Properties of PP sheets made by sheet forming machine are shown in Table II. The name of PP sheets was defined as "resin name," "chill-roll temperature,"—"thickness," for example the sheet named"A80-500" means the sheet with a thickness of 500 μm made from PP-A at a cast at chill-roll temperature of 80°C.

At first the crystallinities of PP sheets were measured. The crystallinity of PP-A and PP-B were almost equal, but the crystallinity increased with increasing the chill-roll temperature from 30 to 80°C [Fig. 3(a)]. The cause of this phenomenon is that the crystallization of PP sheet cast at 80°C was promoted by cooling slowly at a high temperature. In addition, the K-value of A80-500 sheet increased by raising chill-roll temperature, and that corresponds to a result obtained by Fujiyama et al. However, it failed to quantify the *K*-value of A30-500 although existence of the β crystal was confirmed. Although the

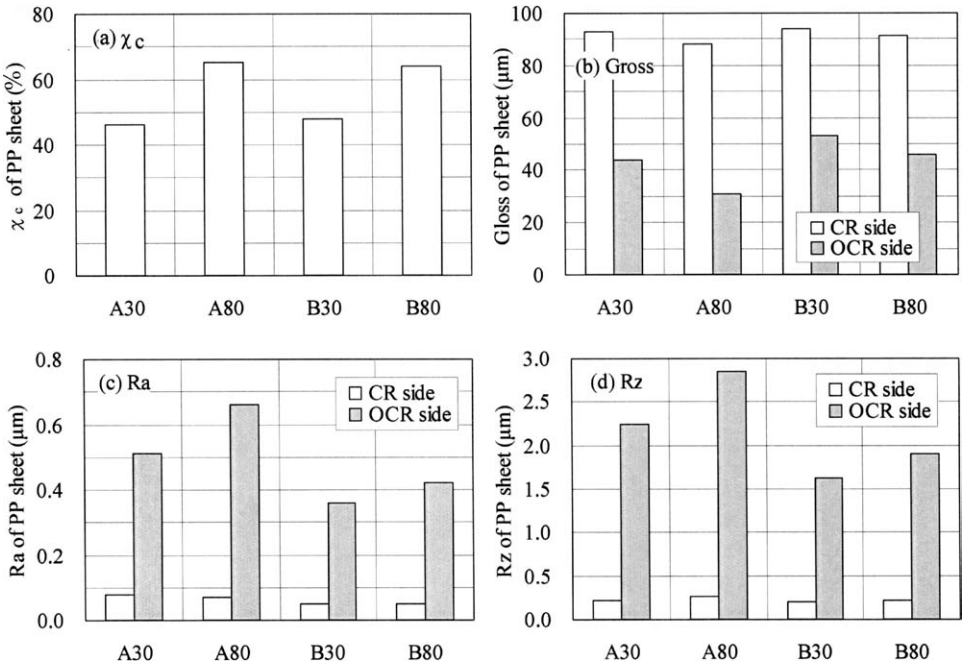

Figure 3 (a) χ_c, (b) gloss, (c) Ra and (d) Rz of PP sheet with different chill-roll temperature. *CR, chill-roll side; OCR, opposite side of chill-roll.

TABLE III
Properties of BOPP Film

Properties		Unit	A30-500f	A80-500f	B30-500f	B80-500f
Stretching temperature		°C	156	156	153	153
Thickness		μm	15	15	15	15
χ_C		%	67	68	61	62
K		–	0.00	0.00	0.00	0.00
Chill-roll side	Ra	μm	0.16	1.46	0.08	0.44
	Rz	μm	0.59	5.43	0.32	1.70
	Gloss	%	122	97	135	104
Opposite side of chill-roll	Ra	μm	0.28	1.29	0.07	0.40
	Rz	μm	1.30	10.3	0.36	2.38
	Gloss	%	121	60	142	73

Other conditions: preheating time; 1 min, stretching ratio; MD/TD = 5/7, stretching speed; 6 m/min.

fact that the (300) peak on X-ray diffractions curves originated from the β crystal of B30-500 was not observed, a very small amount of the β crystal was generated in B80-500 sheet by raising chill-roll temperatures to 80°C.

Then the surface structure of PP sheets was evaluated. When the chill-roll temperature was raised from 30 to 80°C, the glossiness of the opposite side of the chill-roll reduced although the chill-roll side did not show a significant change [Fig. 3(b)]. The glossiness of the PP-A dropped by 13%, and it was more distinctive than that of the PP-B by 7%. The arithmetic mean roughness Ra and 10 points average roughness Rz which were the index of the surface fault degree defined by JIS B0601 [1994] are shown in Figure 3(c,d). Although the sheet roughness Ra and Rz of the chill-roll side were not changed even when the chill-roll temperature was changed, those of the opposite side of the chill-roll increased when the chill-roll temperature was raised. The tendency of PP-A was much more notable compared with PP-B. The reason why the glossiness of the opposite side of the chill-roll of PP-A became lower than that of PP-B was the surface roughness of the opposite side of the chill-roll of PP-A became higher than that of PP-B.

The properties BOPP film stretched using these PP sheets are indicated in Table III. The BOPP film names were defined by putting "f" at the end of PP sheet names, like "A80-500f". The sheets with the PP-B were stretched at 153°C which was 3°C lower than the PP-A sheet stretching temperature because the melting point of the PP-B is 3°C lower than that of PP-A. Crystallinity χ_C of the BOPP films stretched from the sheet cast at 80°C was equal to the one stretched from the sheet cast at 30°C, which showed a different trend to the PP sheet [Fig. 4(a)]. It seems that the influence of the chill-roll temperature disappeared because the noncrystallized part of the PP sheet was easily crystallized by stretching at a high temperature, such as 156°C. The crystallinity of the BOPP films stretched from A80-500 and A30-500 sheets became higher than the crystallinity of B80-500 and B30-500, because the PP-A had a higher stereoregularity than the PP-B.

Figure 4(b) shows the relationship between the glossiness of the sheets and the glossiness of BOPP films. The glossiness of all BOPP films became higher than that of the sheets, as can be seen from the data plotted on the left side of the dotted line. Although the glossinesses of both side of BOPP films

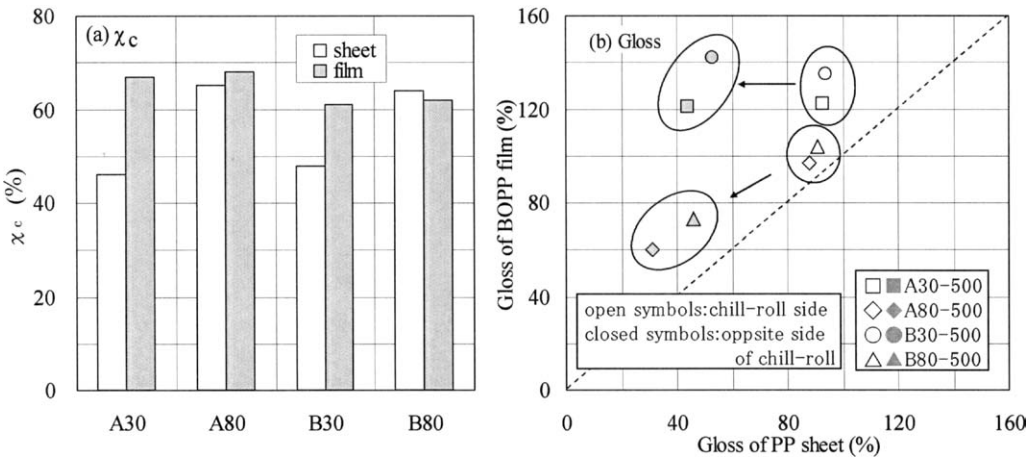

Figure 4 The relationship between PP sheet properties and BOPP film properties, (a) χ_c, (b) gloss.

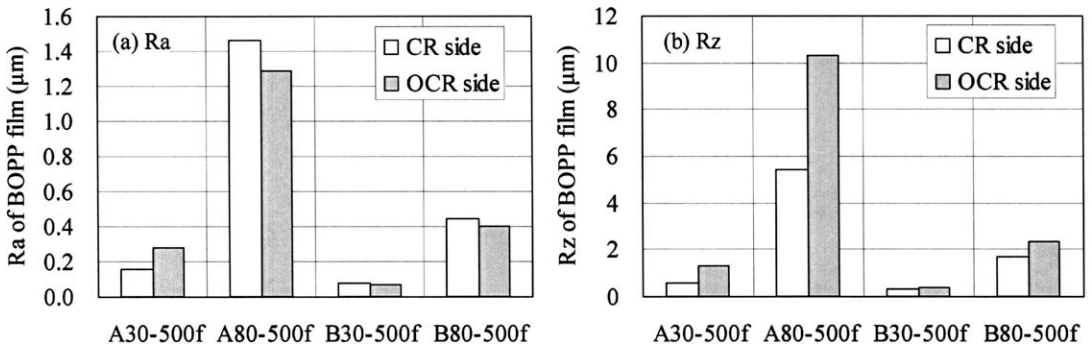

Figure 5 Roughness of BOPP films, (a) Ra and (b) Rz. *CR, chill-roll side, OCR, opposite side of chill-roll.

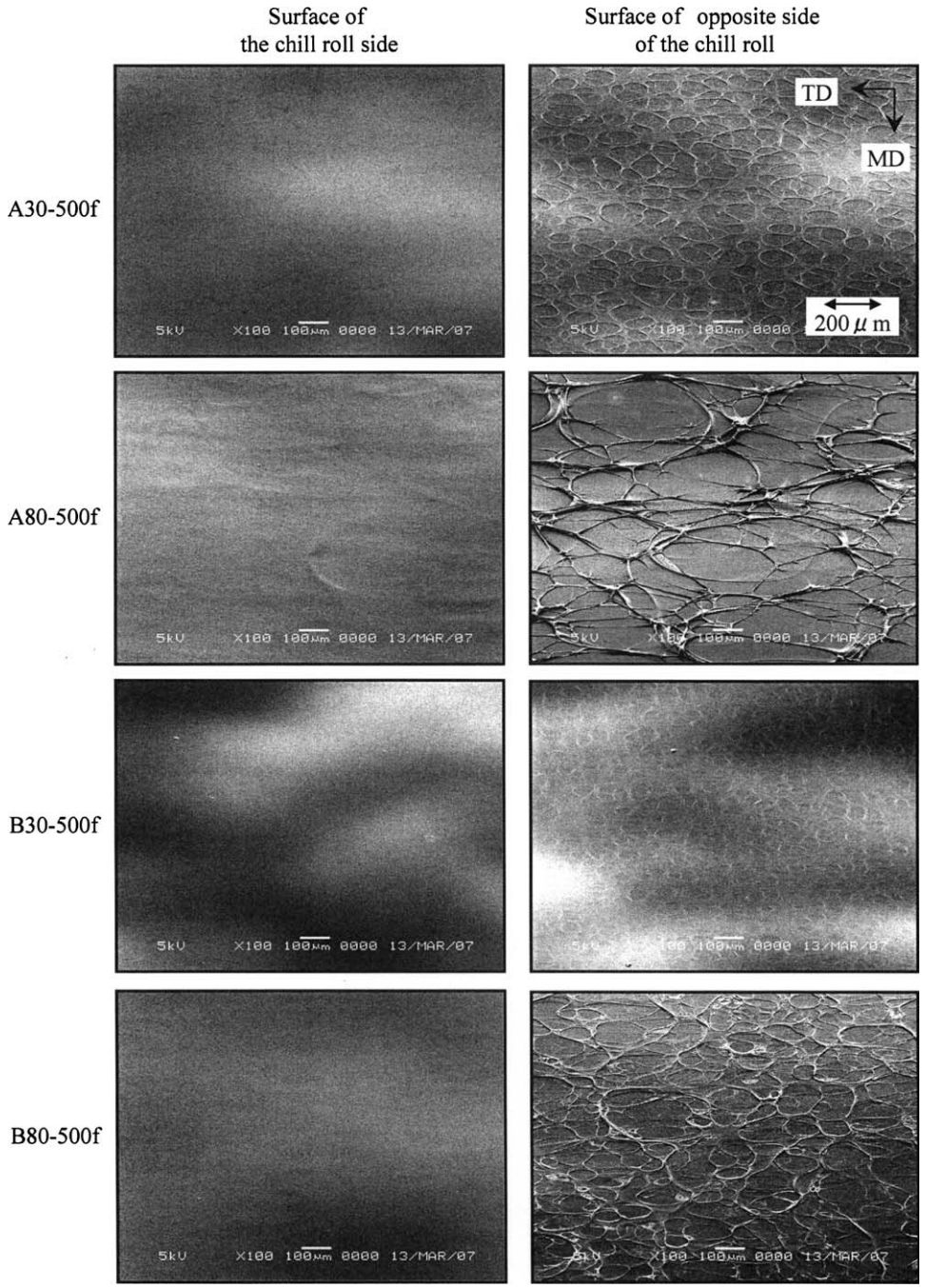

Figure 6 SEM image of BOPP film surface stretched at MD5×TD7 times. (a) A30-500f, (b) A80-500f, (c) B30-500f, and (d) B80-500f.

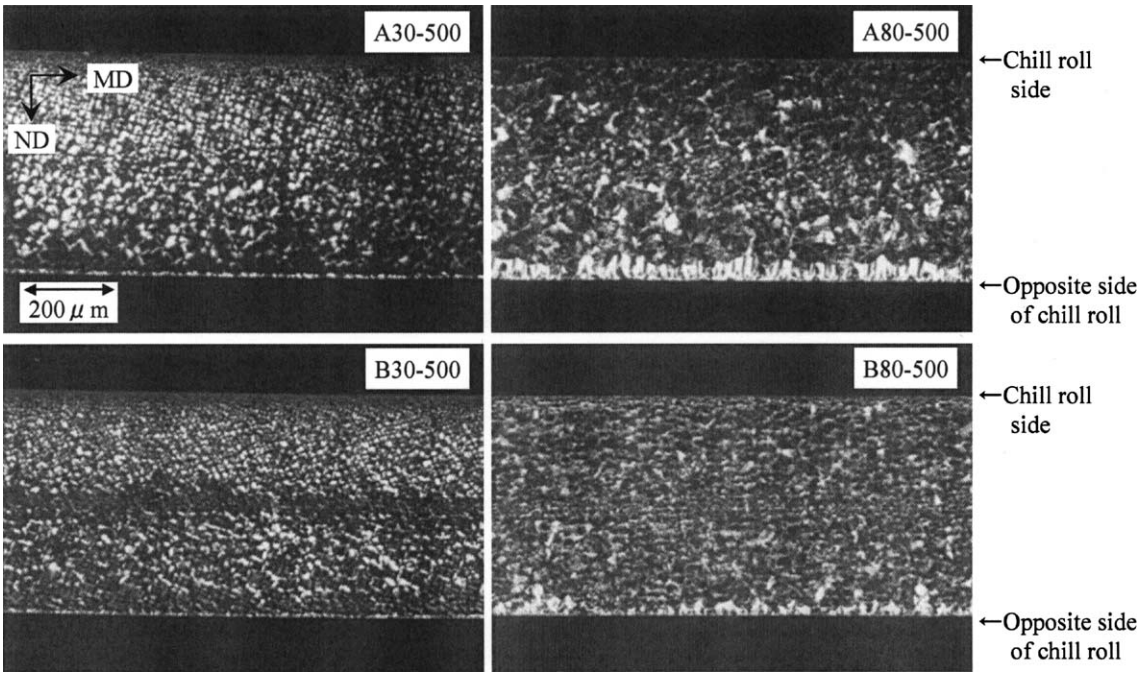

Figure 7 OM image of the cross section of PP sheet.

stretched from the sheets cast at a chill-roll temperature of 30°C were equal, the BOPP film glossiness of the opposite side of the chill-roll cast at 80°C was lower than that of the chill-roll side. This result suggests that the film surface of the opposite side of the chill-roll cast at 80°C becomes rougher than the other surface of BOPP films.

Surface roughness parameter Ra and Rz of BOPP film are shown in Figure 5(a,b), respectively. Both Ra and Rz of BOPP films stretched from the sheets cast at chill-roll temperature of 80°C became higher than those cast at 30°C.

SEM images of the BOPP films' surface are shown in Figure 6. Many crater-like patterns were observed on the BOPP films surface of the opposite side of the chill-roll, but they were not observed on the chill-roll side surface. In addition to that, the A80-500f and B80-500f film surfaces of the opposite side of the chill-roll seemed to be rougher than the other surface. This result corresponds to the glossiness data mentioned in the earlier paragraph. This result also corresponds to the work obtained by Fujiyama et al., and the data indicate that in some cases craters are formed, and in other cases the craters are not formed, which is due to the cooling condition of the chill-roll. In addition, it is shown that the shape of the crater differs remarkably according to the cooling temperatures. The crater size of the BOPP

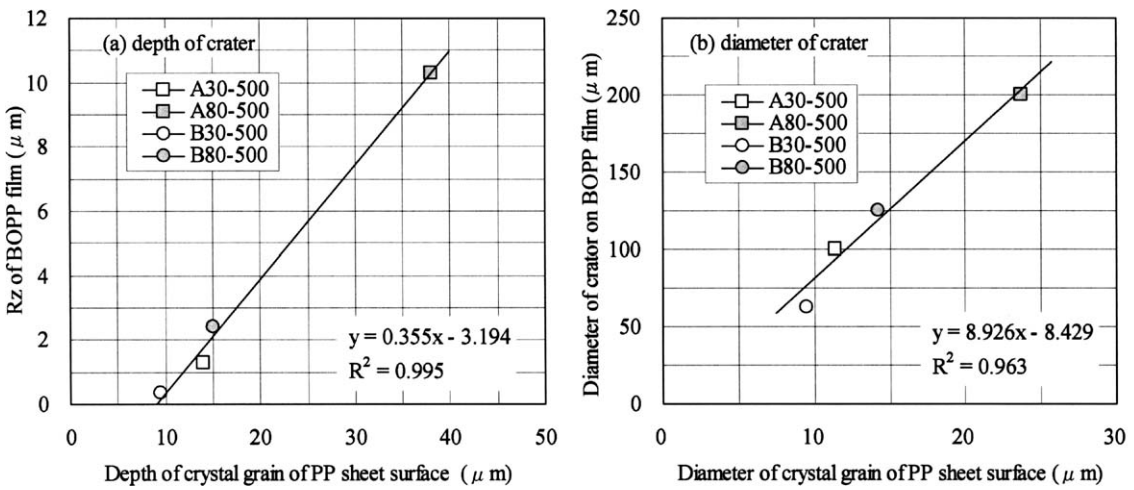

Figure 8 The relationship between the shape of crystal grain on PP sheet surface and shape of craters of BOPP film surface.

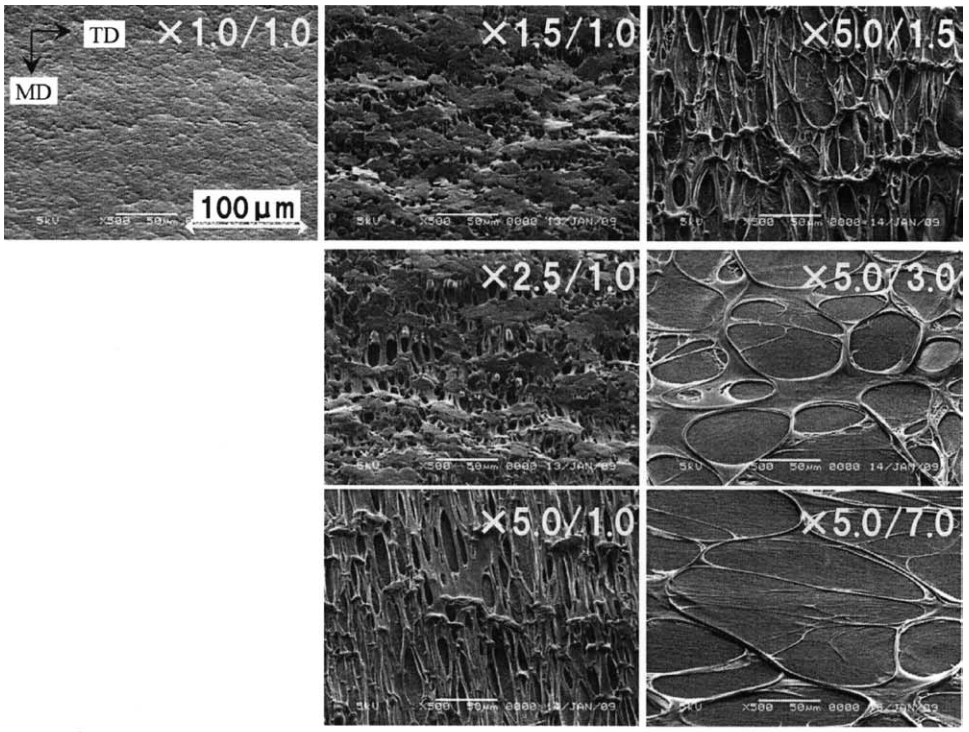

(a) Opposite side of chill roll

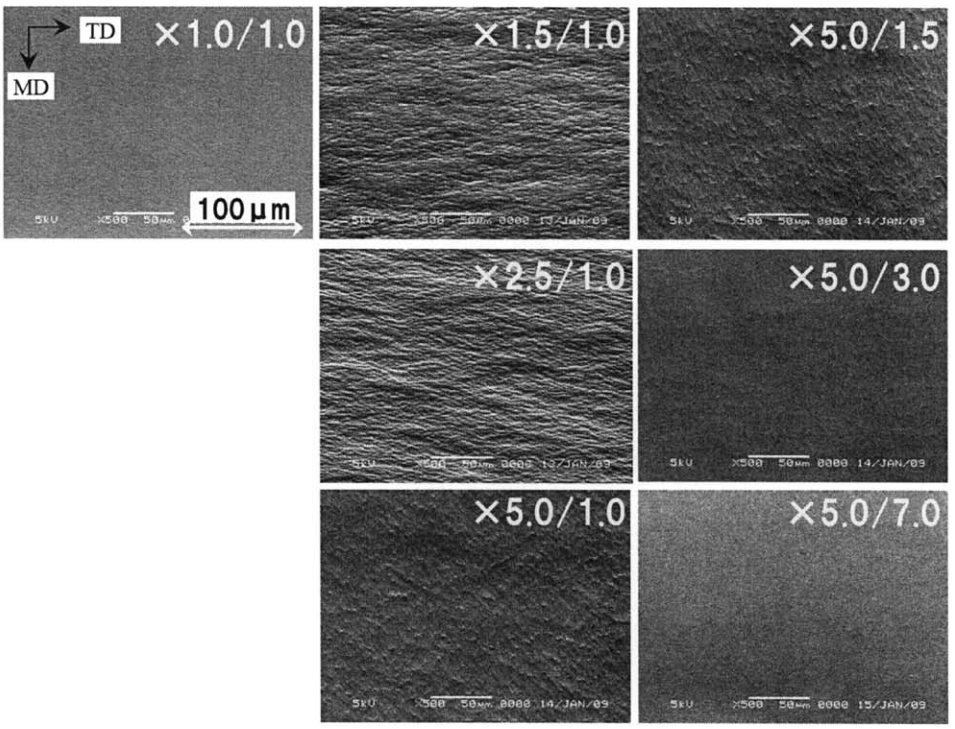

(b) Chill roll side

Figure 9 SEM image of the surface of BOPP film stretched from A80-500 sheet at several stretching ratios at 156°C.

film was larger at the chill-roll temperature of 80°C than at the chill-roll temperature of 30°C. The depth of the crater, which was measured by the height of the wall forming the boundary of the crater, seemed to be higher in the BOPP film stretched from the sheet cast at 80°C than the sheet cast at 30°C. Although the surface of the opposite side of the chill-roll was obviously roughened due to the craters, Ra of the opposite side of the chill-roll of A80-500f and B80-500f indicated lower values than those

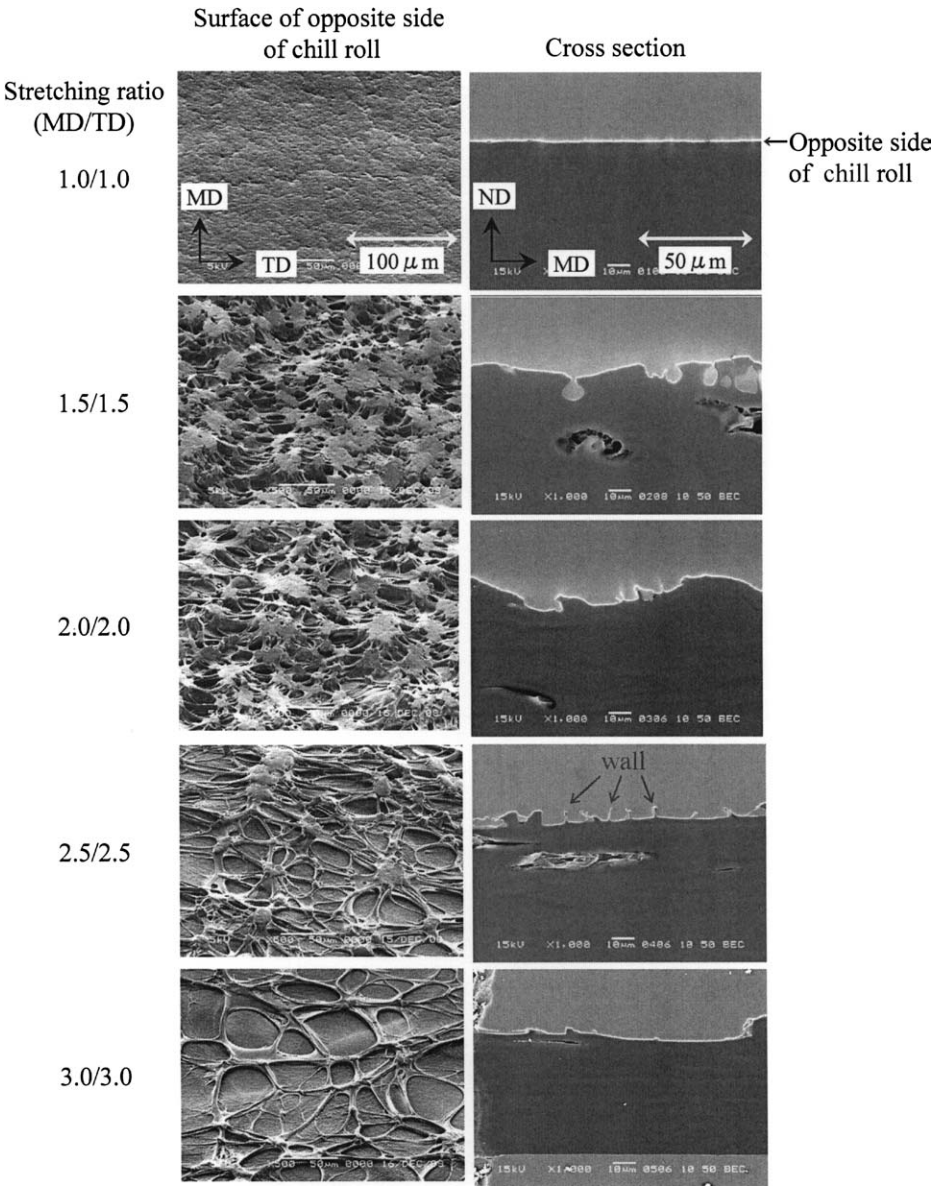

Figure 10 SEM image of the surface of BOPP film stretched from A80-500 sheet at several stretching ratios at 156°C.

of the chill-roll side as shown in Figure 5(a). However, since Rz of the opposite side of the chill-roll was larger than that of the chill-roll side shown in Figure 5(b), and it corresponded with the SEM image, Rz seems to be a good parameter to express the film roughness caused by craters. In this report, Rz was used as the crater depth parameter.

Then, the surface layer structure of PP sheets was observed with an optical microscope using a polarizer, since the cause of the crater's various sizes and depths seemed to be influenced by the different surface structure of PP sheets from the previous analysis. Figure 7 shows the cross-sectional view of PP sheet at the MD and normal direction (ND). As a result, spherulites were confirmed in the central part of the PP sheet as was expected, but there were many white grains in the surface layer of the opposite side of the chill-roll which were not observed in other parts. Since the amorphous parts are not portrayed in white on a polarizing microscope, these white grains are considered to be β crystals of PP from the previous paper.[5] These crystal grains got larger accordingly with the rise of the chill-roll temperature. It is considered that these crystal grains are giving some influence on forming the crater, because they were not observed in the surface layer on the chill-roll side with the temperature at 80°C or lower. After measuring the diameter and the depth of these grains of PP sheet by visual inspection and a diameter and Rz of craters of BOPP films, there seemed to be a good correlation between them (Fig. 8). Therefore, it can be said that the craters were formed from the crystal grains by stretching PP sheets to BOPP films.

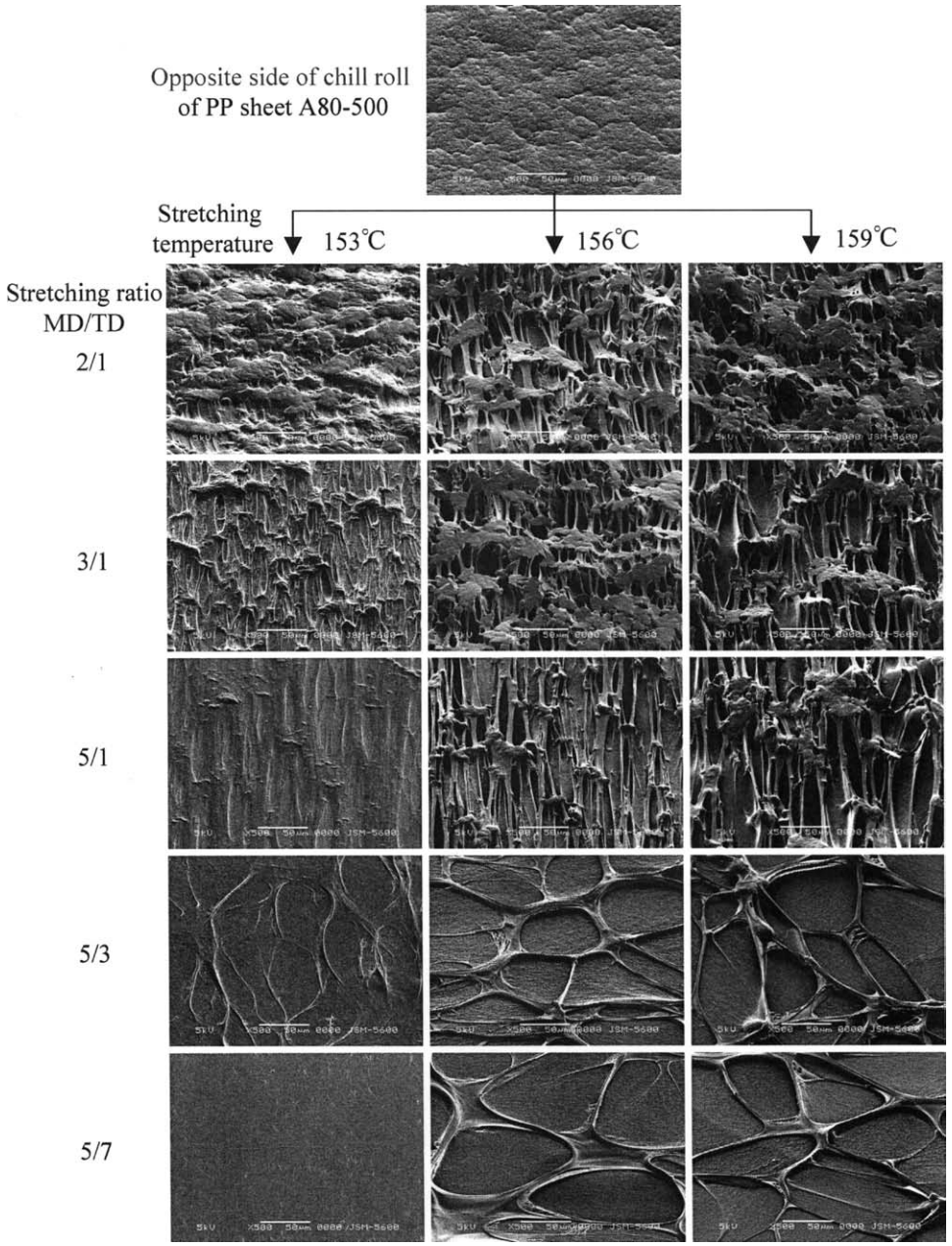

Figure 11 SEM image of the surface of PP film stretched from A80-500 sheet at several stretching ratios and temperatures.

Formation behavior of crater

Formation behavior of the crater was observed with SEM using the PP films at various stretching ratios using a table tenter. On observing the surface structure of the chill-roll side of A80-500, the craters were not found until the BOPP film was stretched at a ratio of 5 × 7 times, even though the film surface was roughened during the middle stretching ratio (Fig. 9). However, a lot of apertures appeared on the surface of the opposite side of the chill-roll after being stretched at only 1.5 times in the machine direction. These apertures became precursors at the beginning of stretching process, and these apertures seemed to grow into craters after the stretching ratio got higher. As a result, craters were produced from the apertures created at the beginning of stretching process as the starting point.

Next, SEM images of the cross-sectional view of PP sheets stretched at arbitrary stretching ratios are shown in Figure 10. Some apertures of around 10–20 μm in depth appeared in the early period of the stretching process at 1.5 × 1.5 times, and the diameter of the aperture increased with increasing stretching ratio. Many thick walls appeared on the stretching ratio at 1.5 × 1.5 times, and at the end the walls between craters were torn apart into thin walls.

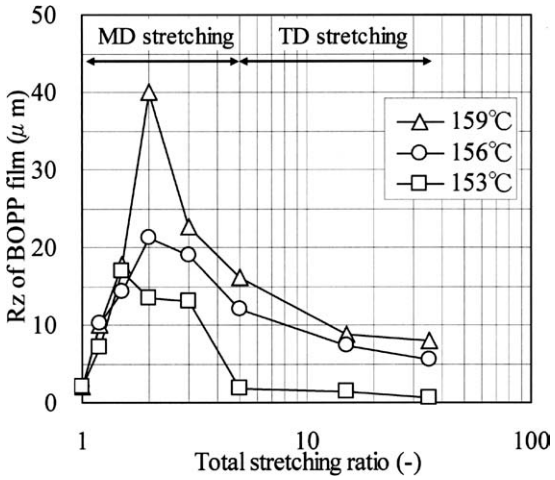

Figure 12 The dependent of surface roughness on total stretching ratio* of A80-500 at several stretching temperatures. *Total stretching ratio = [l(MD) × l(TD)]/ [L(MD) × L(TD)] l(MD), l(TD): length of stretched sample to MD and TD, respectively. L(MD), L(TD): length of initial sample to MD and TD, respectively.

SEM images of crater formation from A80-500 sheet stretched at several stretching temperatures are shown in Figure 11. The depth of the apertures that appeared at the beginning of the stretching process stretched at 153°C was shallower than those stretched at 156°C. After the apertures changed into shallow dent at the MD stretching ratio of three times, very few surface craters were found at the end of the stretching process. Meanwhile, the depth of the apertures that appeared at the beginning of the stretching process stretched at 159°C was deeper than those at 156°C. Finally, deep craters were formed at the end of the stretching process. These results indicate that the stretching temperature is the key factor for the crater shape, because the apertures shape that appeared at the beginning of the stretching process was influenced by the stretching temperature.

Therefore, the effect of the total stretching ratio on Rz of the BOPP film which is a good parameter of the crater depth was investigated in Figure 12. Rz showed a maximum value at a stretching ratio of 2.0, and then got lower as the stretching ratio became larger. After the stretching ratio of 2.0, the size of the crater became larger as the wall between craters were torn. The apertures depth that appeared at the beginning of the stretching process got deeper as the stretching temperature was raised from 153 to 159°C. Therefore, it is believed that there is another crater formation mechanism other than the crystal dislocation system from β crystal to α crystal, because crater shape changed at higher stretching temperature than the β crystal melting point of 148°C.

It is considered that the transformation behavior of this crystal in the surface layer is related to the stretching behavior of the whole film. Figure 13 shows the changes of stretching force with the stretching ratio. A yield points were observed at a stretching ratio of 1.3 and the stretching force gradually decreases at stretching ratios from 1.3 to 5. It is well known that interlamellar separation in the amorphous phase occurs at the beginning of stretching and the spherulite begins to collapse when the stretching ratio passes the yield point.[17–22] Therefore, it is presumed that the grains in the surface layer of the sheet begin to collapse similarly to the spherulites in the middle layer of the sheet. Accordingly, it was assumed that there must be a crater formation mechanism other than the crystal dislocation system related to the collapse of grain in the surface layer.

CONCLUSIONS

In an attempt to clarify the formation mechanism of crater-like surface roughness, different PPs and forming conditions were used in this study. As a result, it was found that chill-roll temperature had a great effect on the shape of the crater and, the crater of the BOPP film stretched from that at 80°C was larger than the PP sheet cast at 30°C. When chill-roll temperature rose, the crystal grain of the PP sheet at surface layer of the opposite side of the chill-roll grew larger. This means that the shape of the crater is closely related to the crystal grain shape.

Furthermore, it was found that the crater grew from the hollow which appeared at the beginning stage of the stretching process. When the stretching temperature was low, the craters were rarely formed at the end of the stretching process because the apertures that appeared at the beginning of the stretching process changed into shallow dents. Meanwhile, craters were formed at the end of the stretching

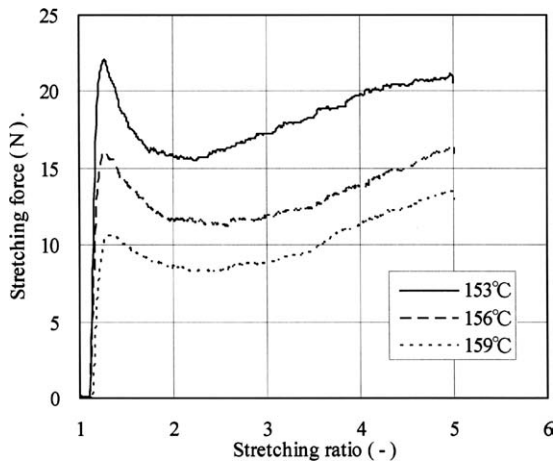

Figure 13 The dependent of stretching force on stretching ratio* of A80-500 at several stretching temperatures. *Stretching ratio = l(MD)/L(MD) l(MD): MD length of stretched sample, L(MD): MD length of initial sample.

process at high temperature because the apertures were deep enough to change into the craters. Finally, it was assumed that there must be another crater formation mechanism related to the collapse of crystalline grain on the surface layer of the sheet other than the crystal dislocation system from β crystal to α crystal.

References

1. Minoda, T.; Kagaku-Keizai. 2009, 3, 88.
2. Ishihara, H.; Shibaya, M.; Yoshihara, N.; Nonomura, C.; Ito, K.; Okudaira, T. J Polym Eng 2005, 25, 81.
3. Fujiyama, M.; Kawamura, Y.; Wakino, T.; Okamoto T. J Appl Polym Sci 1988, 36, 985.
4. Fujiyama, M.; Kawamura, Y.; Wakino, T.; Okamoto, T. J Appl Polym Sci 1988, 36, 995.
5. Fujiyama, M.; Kawamura, Y.; Wakino, T.; Okamoto, T. J Appl Polym Sci 1988, 36, 1011.
6. Fujiyama, M.; Kawamura, Y.; Wakino, T.; Okamoto, T. J Appl Polym Sci 1988, 36, 1025.
7. Fujiyama, M.; Kawamura, Y.; Wakino, T.; Okamoto, T. J Appl Polym Sci 1988, 36, 1035.
8. Fujiyama, M.; Kawamura, Y.; Wakino, T.; Okamoto, T. J Appl Polym Sci 1988, 36, 1049.
9. Fujiyama, M.; Kawamura, Y.; Wakino, T.; Okamoto T. J Appl Polym Sci 1988, 36, 1061.
10. Natta, G.; Gorradini, P. Nuovo Cimento Suppl 1960, 15, 40.
11. Keith, H. D.; Padden, F. J.; Walter, N. M.; Wickoff, H. W. J Appl Phys 1959, 30, 1485.
12. Asano, T.; Fujiwara, Y. Polym J 1979, 11, 383.
13. Meille, S. V.; Ferro, D. R.; Bruckner, S.; Lovinger, A. J.; Padden F. J. Macromolecules 1994, 27, 2615.
14. Moitzi, J.; Skalicky, P. Polymer 1993, 34, 3168.
15. Tuner-Jones, A.; Aizilewood, J. M.; Beckert, D. R. Makromol Chem 1964, 75, 134.
16. Natta, G.; Corradini, P.; Cesari, M. Rend Accad Naz Lincei 1957, 22, 11.
17. Kanai, T.; Yonekawa, F.; Kuramoto, I. 17th Polym. Proc. Society Annu Meeting Abstracts, 17, 2001.
18. Kanai, T. Seikei-Kakou 2006, 18, 53.
19. Kanai, T.; Matsuzawa, N.; Takebe, T.; Yamada, T. Polymer Processing Society Regional Meeting Europe CD-ROM Abstracts, 2007.
20. Kanai, T.; Matsuzawa, N.; Yamaguchi, H.; Takebe, T.; Yamada, T. Europe Regional Polymer Processing Society Annu Meeting CD-ROM Abstracts, 2007.
21. Kanai, T. 24th Polymer Processing Society Annu Meeting CD-ROM Abstracts, 2008.
22. Huy, T. A.; Adhikari, R.; Lüpke, T.; Henning, S.; Michler G. H. J Polym Sci Part B 2004, 42,24, 4478.